FEASIBILITY STUDY ON THE DETERMINATION OF RIPARIAN EVAPORATION IN NON-PERENNIAL SYSTEMS

Colin Everson, Alistair Clulow and Michael Mengitsu

Report to the
Water Research Commission

by

CSIR Natural Resources and the Environment, c/o Soil-Plant-Atmosphere Continuum Research Unit, Agrometeorology Discipline, School of Environmental Sciences, University of KwaZulu-Natal,
Private Bag X01, Scottsville, 3209, South Africa

WRC Project No. TT 424/09

NOVEMBER 2009

Obtainable from:

Water Research Commission
Private Bag X03
Gezina
0031

The publication of this report emanates from a project entitled:
Feasibility Study on the Determination of Riparian Evaporation in Non-perennial Systems
(WRC Project No. K8/775).

ISBN 978-1-77005-905-4

Printed in the Republic of South Africa

Layout: Magdel van der Merwe, DTP Solutions

Contents

Figures

Plates

1. Introduction

Non-perennial river systems are an important source of water in the semi-arid West of South Africa. To date methods of assessing in-stream flow requirements for these river systems with acceptable confidence, i.e. the reserve as required by the National Water Act (1998), have not been developed, despite the fact that people living in the region require an acceptable degree of assurance in their water supply. Methods currently available for the determination of environmental water requirements in South Africa are based on perennial rivers and are seen as needing to be verified for use on non-perennial systems. An important difference in reserve determination between the perennial and non-perennial systems is their different dependencies on the groundwater systems. A study to investigate the changing relevance in ground water in relation to surface water in systems of differing non-perenniality has been undertaken by The University of the Free State (Centre for Environmental Management) and funded by the WRC (Project K5/1587). From these studies the importance of understanding the actual evaporation of riparian vegetation along these non-perennial systems and their link to the ground water systems has been identified as being an important area of research necessary for future management and modelling in these extensive semi-arid regions.

The semi arid Karoo vegetation in the dry regions of the Free State and Eastern Cape form a mosaic of vegetation types dependent on the hillslope position and geology. Three distinct riparian vegetation types can be recognised along the non-perennial streams in the Colesberg area where the UFS studies are being undertaken. These are namely: *1)* Open flat areas in the upper catchment (source area) where the vegetation is dominated by *Juncus* spp *2)* Further downstream (middle reach) there are areas where both *Phragmites* reeds and *Juncus* dominate and *3)* The kloof areas in the lower reaches of the river, where the stream banks are dominated by trees such as *Rhus lancea*. These sites have been chosen to maximize the understanding of the groundwater surface water relationships.

2. Rationale

According to Hughes (2007) it is difficult to infer hydrological processes within a specific catchment without detailed site investigations. He concludes that knowledge of the climate, topography, geology, soils, vegetation and drainage patterns provides important information about the relative importance of the different hydrological processes. In South Africa it is generally accepted that evapotranspiration represents the largest flux in the water balance components of a catchment, with over 80% of the rainfall being lost through evaporative processes. In South Africa there have been no direct measurements of evapotranspiration from non-perennial systems, despite the fact that evapotranspiration in these semi-arid areas is likely to be very high.

One of the most important hydrological processes that have the potential to impact on the ecological functioning of ephemeral river systems is the dynamics of pool storage (Hughes, 2007). In this study it is the evaporative losses from the pool storage component which we

aimed to quantify to assess the difficulty of making evapotranspiration measurements in these complex systems. The main evaporative losses occur as direct evaporation from the pool surface and seepage into the banks of the pool to replenish soil moisture lost through riparian vegetation evapotranspiration (Hughes, 2007). Inputs to pool storage occur from rainfall, surface runoff, groundwater flow (channel bed below the water table), and intermittent interflow in unsaturated zone fractures or intermittent channel flow.

This report describes the evaporation measurements made in early summer (October 2007) and summer (February 2008) over three vegetation types in the Hanover and Colesberg districts of the Karoo.

3. Aim

To estimate early summer and summer evaporation rates from three distinct vegetation types (two riparian and one dryland) along a non-perennial stream for the development of a water assessment methodology.

4. Study Sites

The Seekoei River is situated in the Northern Cape Province. The area experiences summer rainfall with a mean annual total of 300 to 420 mm with a high monthly coefficient of variation of about 1.1. The temperature regime of the region is characterised by large fluctuations in both daily and seasonal temperatures (Venter *et al.*, 1986). Frost is frequent in winter while summer is characterised by hot sunny days due to the generally low cloud cover (annual duration of bright sunshine > 70% of that possible (Schulze, 1965 in Rutherford and Westfall, 1994)). Mean annual potential evaporation is greater than 1900 mm, indicative of the dry, hot semi arid conditions of the karoo. Evapotranspiration in the region is reportedly high with a rainfall deficit between 200 and 220 mm in December (Venter *et al.,* 1986). The topography is generally flat, having a mean catchment slope of 1 to 4%. Steeper gorge areas occur as a result of dolerite ridges, as evidenced in quaternary catchment D32J (Hughes, 2007). The gorge area is expected to have very different hydrological response characteristics to the rest of the catchment (Hughes, 2007). The vegetation cover is very sparse and is described as shrubland with low Fynbos, except in the channel margins where larger trees and shrubs grow as a result of their improved access to sub-surface water.

After a preliminary site visit to the area with Dr Maitland Seaman and Prof Dennis Hughes, it was decided to investigate the Upper reaches of the Seekoei River in the proximity of EWR site 1 and in the gorge area represented by EWR site 3 (EWR = Ecological Water Requirement). The short fynbos vegetation adjacent to the phreatic zone at EWR site 1 was included as a separate site to act as a control and provide further information on the evapotranspiration from this "dryland" vegetation.

4.1 Upper Reach of the Seekoei River – EWR Site 1

The site falls within quaternary catchment D32E and has a reach length of 35 km. The site was located on the farm Vanzylskraal about 20 km south west from Hanover. The in stream and riparian zone are described as being largely natural by Watson and Barker, 2006 cited in Avenant, 2006 (IHI and RHI class B respectively).

In mid-October 2007 the dryland vegetation along side the phreatic zone was approximately 0.20 m tall and had an estimated aerial cover of < 30%. At this time there had been no significant rainfall for seven of years (T.C. Niewhoudt *pers comm*.) and most of the vegetation appeared dead (Plate 4.1). The area was being heavily utilised by sheep during this period. Following good rainfall in December and January the site had recovered significantly by the time of the summer field campaign (Plate 4.2). By this time the vegetation was 0.30 m tall and the aerial cover was estimated to be > 70% (Plate 4.2).

The riparian vegetation at EWR site 1 was characterised by a narrow strip of 1.5 m tall *Juncus* spp (tall sedge) which appeared mostly dormant from the large percentage of grey material in the canopy (Plate 4.3). By February the sedge canopy had greened up significantly (Plate 4.4). There was also evidence of newly emergent *Phragmites* reeds.

4.2 Lower reach of the Seekoei River – EWR Site 3

The study site for EWR 3 is located on the farm Holfontein about 15 km north west of Colesberg in quaternary catchment D32J. The vegetation on the steam banks consists predominantly of tall Willow trees, *Rhus lancea, Acacia karoo*, *Phragmites* and *Juncus* spp. The river in the valley bottom point is wide (>25 m) and is bounded by steep dolerite cliffs on either side of the valley (Plates 4.5 and 4.6).

Two field campaigns were made. The early summer trip was from the 12th to 22nd of October and the summer campaign was from 4th to 14th of February 2008. The objective was to obtain a representative time series of the energy balance components of the three selected vegetation communities to test the feasibility of using the applied technologies for measuring evaporation in these technically demanding sites, where advective effects could possibly be extreme due to the impacts of the surrounding extensive semi-arid vegetation.

Plate 4.1. Condition of the "dryland" karoo shrubland at the EWR site 1 in October 2007 following a prolonged drought. Note the low aerial plant cover.

Plate 4.2. Condition of the "dryland" karoo shrubland at the EWR site 1 in February 2008 following good rainfall in the area. Note the high aerial plant cover.

Plate 4.3. The phreatic zone at EWR site 1 in October 2007. The riparian vegetation was dominated predominately *Juncus* spp.

Plate 4.4. The phreatic zone at EWR site 1 in October 2007.

Plate 4.5. The study site at EWR 3 on the farm Holfontein in the Colesberg district. The LAS 150 receiver can be seen in the foreground.

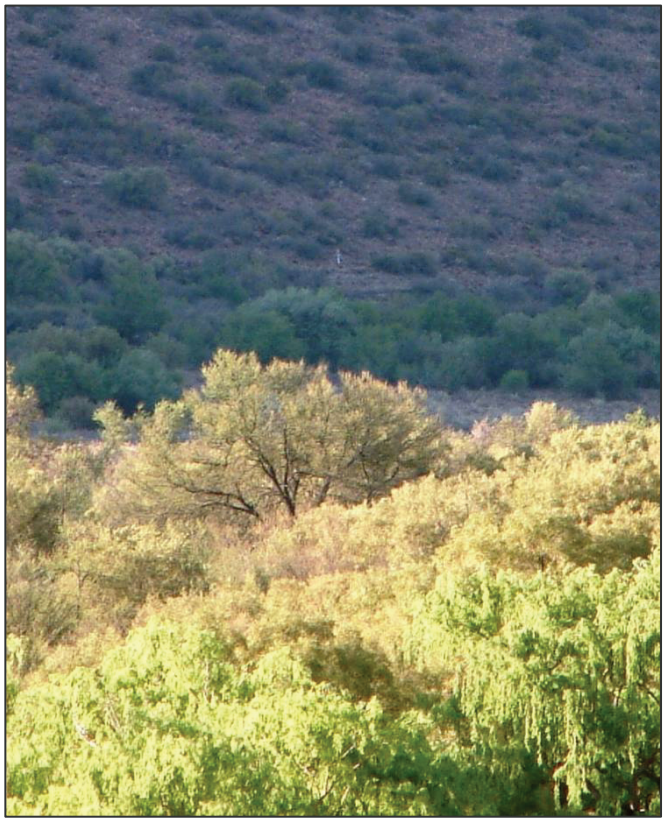

Plate 4.6. The study site at EWR 3 on the farm Holfontein in the Colesberg district. The LAS 150 transmitter can just be seen in the background.

5. Measurement systems

Two different measurement systems were applied in this study to obtain direct measurements of the evaporation and energy balance components of the three different vegetation types. A large aperture scintillometer was used at EWR 3 since it was best suited to the long transect (1120 m) at this site. The second type of scintillometer system used was surface layer scintillometers which were better suited to the short transects (< 200 m) at the EWR 1 site.

Most of the micrometeorological methods used to estimate evapotranspiration are ultimately based on the energy balance equation, which accounts for all losses of energy that are available for vaporising water. The shortened energy balance equation is expressed as:

$R_n = F_g + F_h + \lambda E$	*5.1*

where R_n is the net irradiance, F_g is the soil heat flux density, F_h is the sensible heat flux density, and λE is the latent energy flux density. Since there are few easy methods for directly measuring λE, it is usually determined as the residual in Equation 5.1 by measuring R_n, F_g and F_h. The available energy is calculated by re-arranging the shortened energy balance equation (Equation 5.1), to $R_n - F_s = L_v F_w + F_h$ where $R_n - F_s$ is the available energy. For any day, the magnitude of the latent heat flux ($L_v F_w$) is then equal to the flux between the available energy and F_h.

5.1 Introduction

A scintillometer is an instrument designed for optically measuring the path-averaged structure parameter of the refractive index of air (C_n^2) over horizontal path lengths. It consists of a transmitter or light source of known wavelength directed towards a receiver. The receiver measures intensity fluctuations in the beam from the transmitter. These fluctuations are called scintillations and are caused as a result of weak refractive scattering by turbulent eddies between the transmitter and the receiver. Changes in air temperature change the refractive index of air, causing scattering. The refractive scattering is produced predominantly by atmospheric perturbations caused by fluctuations in sensible heat that refract the light beam. The structure parameter of the refractive index of air (C_n^2) is thus a measure of the turbulent strength of the atmosphere causing scintillations of the light beam from the transmitter.

There are a number of different types of scintillometers. The large aperture scintillometer (LAS) was developed in the 1970s (Wang *et al.*, 1978). The LAS is defined by the size of the aperture, which is 0.152 m, and the optical wavelength of 880 nm. Savage *et al.* (2004) describe the theory of the Fresnel Zone explaining the difference between the Surface Layer Scintillometers (SLS), the LAS, and the Boundary Layer Scintillometer (BLS). The SLS has a small aperture and is sensitive to small eddies of about 12.9 mm which would occur closer to the ground surface. It has a pathlength of 80 to 250 m. The LAS is sensitive to eddies of about 68.6 mm and can operate between 2.5 and 4.5 km. The BLS is sensitive to eddies up to 93.8 mm and operates at path lengths in the 0.5 to 8 km range (Savage *et al.*, 2004; Kipp and Zonen, 2007; Odhiambo, 2007).

5.2 Principles of Scintillometry

The theory of scintillometry is a complex subject requiring a good understanding of electromagnetic wave propagation, the structure of the atmosphere and meteorology to mention a few. It is beyond the scope of this project to review all the theory of scintillometry and we therefore only attempt to give the reader enough background to understand how the sensible heat flux (F_h) was derived in this study using the LAS and SLS data.

The receiver is sensitive to the structure parameter of the refractive index of air, C_n^2. This is in turn linked to the structure function parameter for air temperature, C_T^2 which is then linked to a derivation of the sensible heat flux. The parameter C_n^2 can be seen as the 'turbulent strength' of the atmosphere which describes the ability of the atmosphere to transport scalars such as sensible heat flux.

The relationship between the measured variance of the natural logarithm of intensity fluctuations logged at the receiver and the structure parameter is:

$$C_n^2 = 1.12\,\sigma_{lnI}^2\,D^{\frac{7}{3}}\,L^{-3} \qquad 5.2$$

where C_n^2 is the structure parameter of the refractive index of air, σ^2_{lnI} is the variance of the logarithm of amplitude fluctuations, D is the aperture diameter (m), and L is the beam path length (m).

Air temperature and humidity cause air density fluctuations which result in fluctuations in C_n^2. In this way C_n^2 is divided into the structure parameters of temperature (C_T^2), relative humidity ($C_Q{}^2$) and a covariant term C_{TQ}. As a simplification, Wesley (1976) showed that for a LAS, operating at a near-infrared wave length, C_n^2 is related to $C_T{}^2$ as follows:

$$C_T^2 = C_n^2\left(\frac{T^2}{-0.78\times10^{-6}P}\right)^2\left(1+\frac{0.03}{\beta}\right)^{-2} \qquad 5.3$$

where C_T^2 is the structure parameter of temperature, T is the absolute air temperature (K), P is the atmospheric pressure (kPa), and β is the Bowen ratio. The Bowen ratio is commonly used in micrometeorology and is defined as:

$$\beta = \frac{F_h}{L_v F_w} \qquad 5.4$$

The final step in the determination of F_h is to establish the link with C_T^2. This link is derived from the Monin-Obukhov Similarity Theory (MOST) (Wyngaard *et al.*, 1971). Only the unstable solution will be considered for which the Obukhov length (L_{Ob}) is negative:

$$\frac{C_T^2 (z_{LAS} - d)^{2/3}}{T_*^2} = f_T\left(\frac{z_{LAS} - d}{L_{Ob}}\right) \qquad 5.5$$

where z_{LAS} is the scintillometer height above the surface (m), d is the zero plane displacement height (m), T_* is the temperature scale of turbulence (K) and f_T is the universal stability function.

L_{Ob} represents the thickness of the layer of dynamic influence near the surface in which shear or friction effects are always important. Meijninger *et al.* (2002) define L_{Ob} mathematically as:

$$L_{Ob} = \frac{u_*^2 T}{gkT_*} \qquad 5.6$$

$$\textbf{where } T_* = \frac{-F_h}{\rho_a c_p u_*} \qquad 5.7$$

$$\textbf{and} \qquad u_* = \frac{ku}{\ln\left(\frac{z-d}{z_o}\right) - \psi_m\left(\frac{z-d}{L_{Ob}}\right)} \qquad 5.8$$

where u_* is the friction velocity (m s^{-1}), g is the gravitational acceleration (m s^{-2}), k is the von Karman constant, u is the horizontal wind speed (m s^{-1}), z is the height of the wind speed measurement (m), z_o is the roughness length (m) [≈ 0.1 times the canopy height], and Ψ_m is the Businger-Dyer correction for stability.

In a horizontally homogeneous surface layer, the mean flow and turbulent properties are dependant on four independent variables namely: the height above the surface (z), the friction velocity (u_*), the surface kinematic heat flux ($F_h/\rho_a c_p$), and the buoyancy variable (g/T_o) where T_o is the surface temperature (Monin and Obukhov, 1954).

In summary, C_n^2 data together with air temperature, wind speed, surface roughness and displacement height, are used to calculate F_h by solving the equations above iteratively for a known function f_T.

The following data were required to compute sensible heat flux for the LAS:

- mean of C_n^2 (measured as UCN2 on the logger),
- mean of signal strength (Udemod),

- variance of signal strength,
- path length,
- effective beam height,
- zero displacement height,
- atmospheric pressure,
- air temperature,
- horizontal wind speed,
- Bowen ratio,
- height of anemometer and
- surface roughness.

The SLS systems, although based on much of the above theory, are computationally more advanced and only the path length and effective height were required as additional inputs.

5.2.1 Determination of Effective Height

The ability of the LAS to be able to determine fluxes at large scales is particularly attractive to modellers that need area average fluxes as inputs or verifications. Hydrological studies often need fluxes at catchment scales and remote sensing techniques need fluxes at satellite pixel scale. For this reason scintillometers are frequently used over heterogeneous and non-flat terrain where non-ideal situations are encountered.

Along an extended transect the LAS may be installed over valleys or buildings which may result in a slanted scintillometer beam. Where a scintillometer beam height varies or is slanted, the measurements represent not only a horizontal, but also a vertical average of C_T^2. The average height of the beam along the path length does not represent the height of the vertically averaged C_T^2 because C_T^2 does not vary linearly with height. To complicate matters further, the sensitivity of the scintillometer is weighted towards the middle of the beam for equally-sized transmitter and receiver.

Hartogensis *et al.* (2003) stresses the sensitivity of F_h to z_{LAS} (the LAS height) for unstable conditions. They show that for free convection conditions, a relative error in z_{LAS} causes an equal relative error in F_h. For neutral conditions, a relative error in F_h due to z_{LAS} is half the relative error in Z_{LAS}. The fact that F_h is so sensitive to z_{LAS} shows the importance of determining z_{LAS} as accurately as possible. This emphasises the importance of deriving an accurate estimate of effective height where the LAS beam is not at a constant height above the ground.

Hartogensis *et al.* (2003) was able to derive a lengthy equation for effective height but was able to simplify it for certain conditions if the variation along the path is relatively small. The original equation can be simplified in three ways according to site and temporal conditions. The first considers either neutral or free convection conditions. For the effective height of the beam for free convection, Z_{eff_Fc} (m), for which $z_{LAS}/ L_{Ob} \rightarrow \infty$, is defined by:

$$Z_{eff\_Fc} = \left(\int_0^1 Z(u)^{-\frac{4}{3}} G(u)\, du \right)^{-\frac{3}{4}} \qquad 5.9$$

where $Z(u)$ is the scintillometer beam height along the path (m), $G(u)$ is the weighting function describing the contribution of $C_T^2(u)$ at each point along the normalised path, u, to the total LAS weighted C_T^2.

For the neutral case ($z_{LAS}/ L_{Ob} \rightarrow 0$):

$$Z_{eff\_Fc} = \left(\int_0^1 Z(u)^{-\frac{2}{3}}\, G(u)\, du \right)^{-\frac{3}{2}} \qquad 5.10$$

The second approximation assumes that the influences of stability and height dependency of the original equation are negligible and in the calculation of $Z_{eff\_WeightAvg}$, $Z(u)$ is weighted with weighting function $G(u)$:

$$Z_{eff\_WeightAvg} = \int_0^1 Z(u)\, G(u)\, du \qquad 5.11$$

In the third approximation, the scintillometer weighting function, $G(u)$ is left out of consideration leaving:

$$Z_{eff\_Avg} = \int_0^1 Z(u)\, du \qquad 5.12$$

In this study we used the average of the results from Equations 5.11 and 5.12 to calculate the final effective height.

5.2.2 Roughness Length and Zero Plane Displacement

A number of the equations involving MOST require estimates of the zero plane displacement (Equation 5.6) and roughness length (Equation 5.8). These parameters are usually found by fitting a logarithmic wind profile equation to measured wind profiles. It is now well received that the horizontal wind speed variation with vertical height under neutral stability obeys the semi-logarithmic law (Monteith and Unsworth, 1990):

$$\frac{u_z}{u_*} = \frac{1}{k} \ln\left(\frac{z-d}{z_0} \right) \qquad 5.13$$

where u_z is the horizontal wind speed at height z (m s^{-1}).

Using Equation 5.13, Rosenberg *et al.* (1983) describe how it is possible to solve for d and z_o with wind profile measurements. Measuring wind profiles is however inconvenient especially at a catchment scale where roughness length and zero plane displacement heights are variable. For this reason attempts have been made to relate them to easily measurable properties of the earth's surface. Early attempts were made to define them according to a fraction of the vegetation height. Typically it was found that z_o = 0.13 h and d = 0.66 h, where h is the average height of the vegetation (Verhoef *et al.*, 1997). More recently Kipp and Zonen (2007) recommend values of 0.1 h and 0.67 h for surface roughness and zero plane displacement respectively.

6. Materials and Methods

6.1 Instrumentation at EWR Site 1

We deployed two OEBMS1 systems at the site. The OEBMS1 is a complete system to measure surface energy budgets. Unlike conventional stations, the OEBMS1 uses optical scintillation to obtain the turbulent heat flux. The result gives high accuracy even with short averaging periods: while conventional stations need averaging times of 30-60 min, the OEBMS1 resolves all components in two minute steps – virtually without statistical scatter and representatively characterizing large experimental areas.

Each OEBMS1 consisted of one SLS40A scintillometer system with tripods to measure the sensible heat flux, one pyrradiometer (0.3-30 µm) and one pyranometer (0.3-3 µm) to measure the radiation flux balance, and three soil heat flux sensors (new circular design for minimum heat flow disturbance). The latent heat flux was calculated as the residuum of the other components. Two ventilated thermometers Pt100 and one pressure sensor provided the auxiliary data for an automatic derivation of the turbulent heat flux from the scintillation measurements (Plate 6.1). The beam direction of the system over the riparian area was 38° East of North and 91 meters long, while the dry veld transect was 36° West of North and 94 meters long. The two OEBMS1 systems were setup in identical positions in October 2007 and February 2008 (pegs were left in the ground to aid in the relocation of the various instruments).

The OEBMS-SPU1 Signal Processing Unit interfaces with all sensors and communicates with a PC via an RS232 line. The software OEBRUN on the PC outputs the following components:

- turbulent flux of sensible heat
- turbulent flux of latent heat (evaporation)
- incoming solar radiation and net radiation (solar plus thermal)
- ground heat flux (average over 3 sensors and individual values).

A diagrammatic representation of the equipment is shown in Figure 6.1.

Plate 6.1. The OEBMS1 mast with pyrradiometer, pyranometer, soil heat flux sensors and two ventilated thermometers (Pt100) at the EWR 1 site. Phote taken in February 2008.

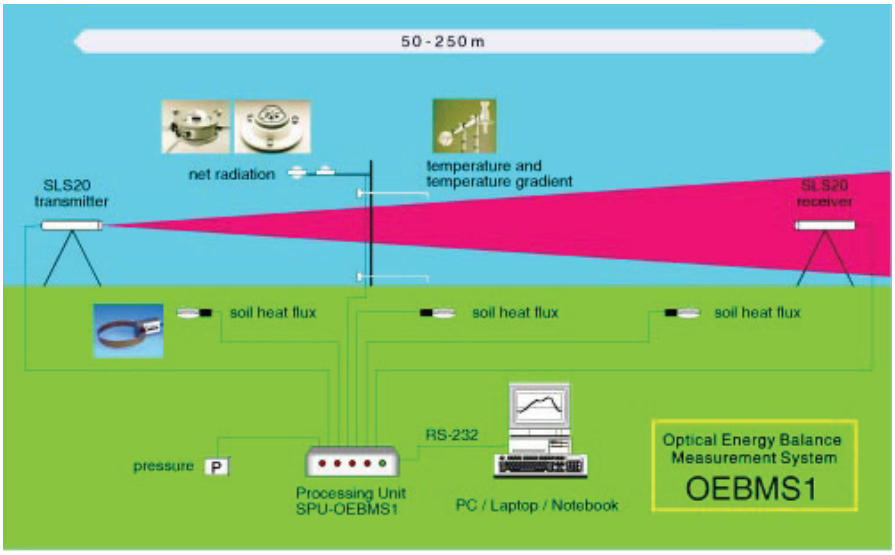

Figure 6.1. Diagrammatic representation of the OEBMS1 system as setup at Hanover in February 2008 (Diagram courtesy of Scintec).

The two OEBMS1 systems were setup in identical positions in October 2007 and February 2008 (pegs were left in the ground to aid in relocation of the position of the various instruments). The dry veld and riparian zone OEBMS1 systems are shown in Plates 6.2 & 6.3 respectively.

Plate 6.2. The setup of the dry veld OEBMS1 system (October 2007). The transmitter laser beam can be seen shining in the background.

One disadvantage of the OEBMS1 systems was that they have a large power requirement. To overcome this problem an "intelligent" self starting petrol generator controlled by a CR23X datalogger was used to power two 40 Amp battery chargers, each charging 4 RR2 100 Amp hour batteries. The two laptop computers running the SLS Run 3.2 software were powered by two 12 V to 220 V inverters. The entire battery system plus the signal processing units, junction control boxes and laptop computers were housed in an off road trailer which was left at the site (Plate 6.4). With this system the batteries lasted for approximately 7 hours. When the datalogger sensed the voltage dropping below 12.4 V the batteries were recharged for two hours. The modified fuel tank (25 *l*) required filling approximately every five days.

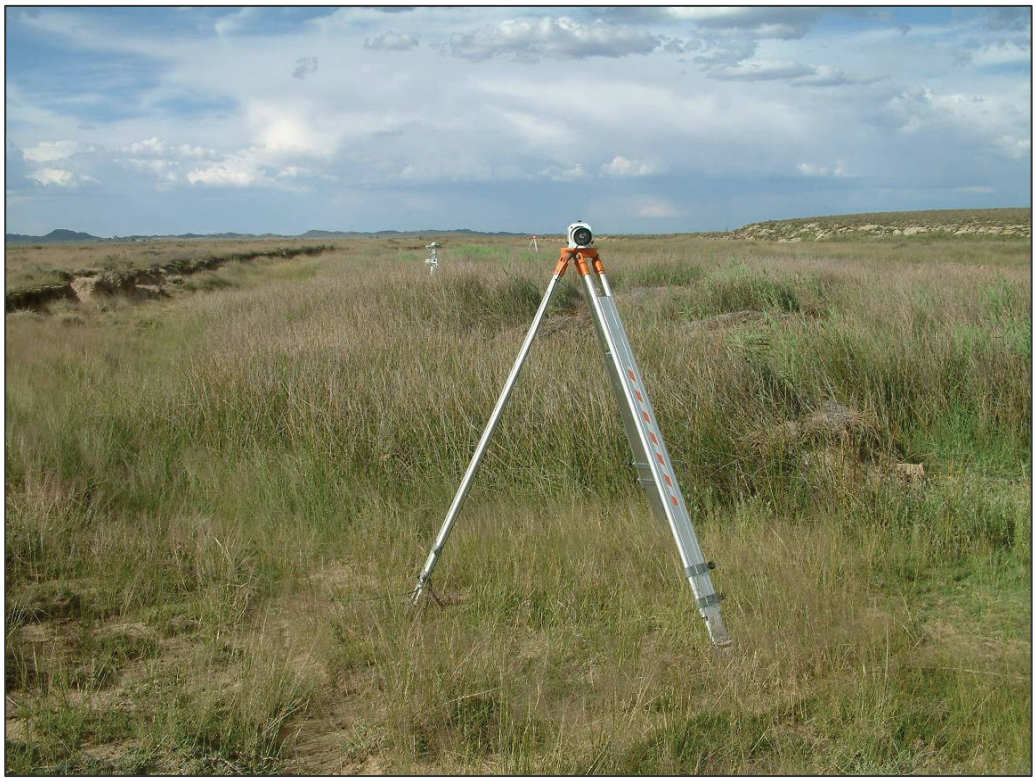

Plate 6.3. The setup of the riparian zone OEBMS1 system (February 2008).

Plate 6.4. The specially designed petrol generator (left) and the battery chargers, invertors and two banks of four RR2 100 Amp hour batteries (right) used to power the two OEBMS1 systems.

6.2 Instrumentation at EWR Site 3

6.2.1 LAS instrumentation

At the EWR 3 site, a suitable location was found with a path length of 1120 m with a North-South orientation. The transmitter was situated at the northern end of the transect.

A Garmin GPS was used to derive a topographical profile description of the site (Figure 6.2). The canopy height of the vegetation was also measured at approximately 30 m intervals along the transect. The effective height of the beam above the plant canopy was calculated to be 11.5 m. Superimposed on Figure 6.2 is a bell-shaped function that illustrates the relative sensitivity of the measurements along the transect.

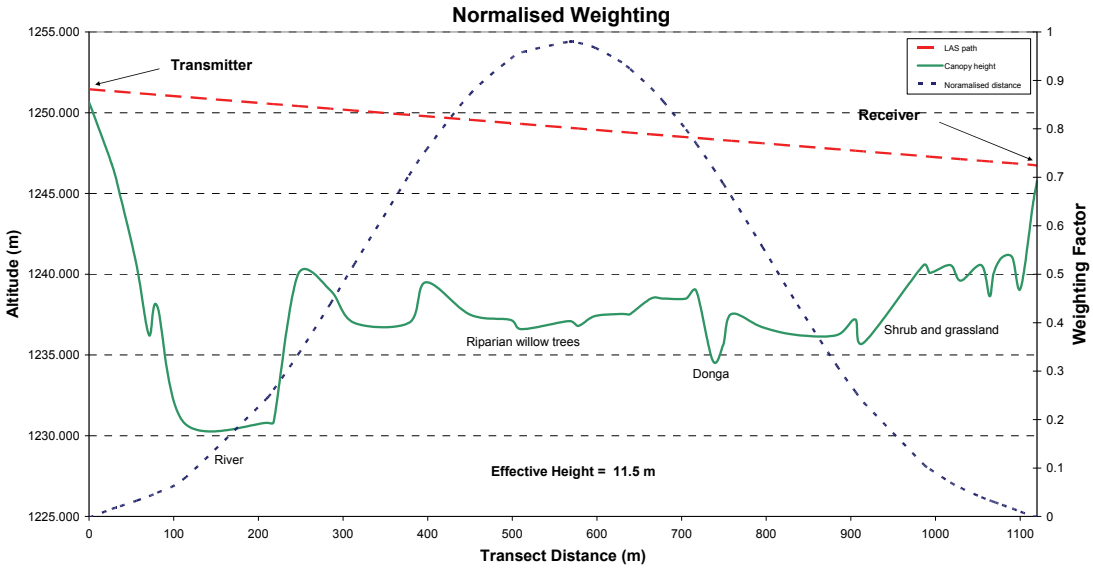

Figure 6.2. Topographical profile of the canopy surface along the LAS transect; also showing the path of the scintillometer beam and the normalised weighting curve used in the calculation of the effective height.

The LAS used at EWR 3 was manufactured by Kipp and Zonen. The light source of the transmitter operated at a near-infrared wavelength of 880 nm. At this wavelength, the observed scintillations are caused primarily by turbulent temperature fluctuations. The carrier beam is 7 kHz and the aperture diameter is 0.152 m.

Power was supplied by single 100 A h batteries to both the transmitter and the receiver. This was sufficient power for the duration of the field campaign.

Rifle telescopes mounted on each LAS unit were used to assist in the beam alignment. A signal strength meter at the back of the receiver gave an indication of alignment. The transmitter and receiver units were controlled by panning and tilting the units by operators at both ends communicating with two-way radios until the maximum signal strength was obtained.

The signal strength on the transmitter and path length potentiometer on the receiver was set to appropriate values and the user manual gave an indication of suitable ranges. The path length values on the dial of the receiver are not in meters but in relative units.

A Campbell Scientific CR23X logger was used to log the data from the receiver LAS. The data, based on input measurements every second, were averaged every 10 min and stored in the logger memory. The Winlas software was used to process the LAS output, C_n^2, together with the horizontal wind speed, air temperature, air pressure and Bowen ratio (Kipp and Zonen, 2007). The processed file includes a stable and unstable solution of sensible heat. The unstable solution was used during the day-time when net irradiance was positive. At night, when the stable solution was used to determine F_h, zero evaporation was assumed. L_vF_w was calculated as a residual of the energy balances and converted to ET.

6.2.2 Energy Balance Weather Station

Net irradiance, soil heat flux and horizontal wind speed above the canopy were required for the calculation of the latent energy flux using the Winlas software and the shortened energy balance (Equation 5.1). In addition, wind direction, relative humidity and air temperature were also measured at the site for completeness. The FAO 56 short grass reference evaporation was computed online by the logger. Table 6.1 shows the details of the measurements. Figure 6.4 shows the instrumentation of the energy balance weather station site.

Table 6.1. Sensors and measurements at the energy balance weather station (scan rate of 10 s and an output interval of 10 min and daily).

Sensor	Measurement	Location
RM Young wind sentry	Wind speed and wind direction	1.5 m above canopy
Vaisala CS500	Relative humidity and air temperature	1.25 m above canopy
REBS Q*7.1 Net radiometer	Net irradiance	1.25 m above canopy
Soil temperature averaging probes	Soil temperature	20 and 60 mm below soil surface
REBS soil heat flux plates	Soil heat flux	80 mm below soil surface
Texas Instruments raingauge	Rainfall (0.1 mm resolution)	0.1 m above canopy

Figure 6.3. The EWR 3 energy balance and weather station site.

The soil heat flux plates were installed at the base of the mast under the *Acacia karoo* canopy. A representative area was chosen and the sensors were installed as shown in Figure 6.4.

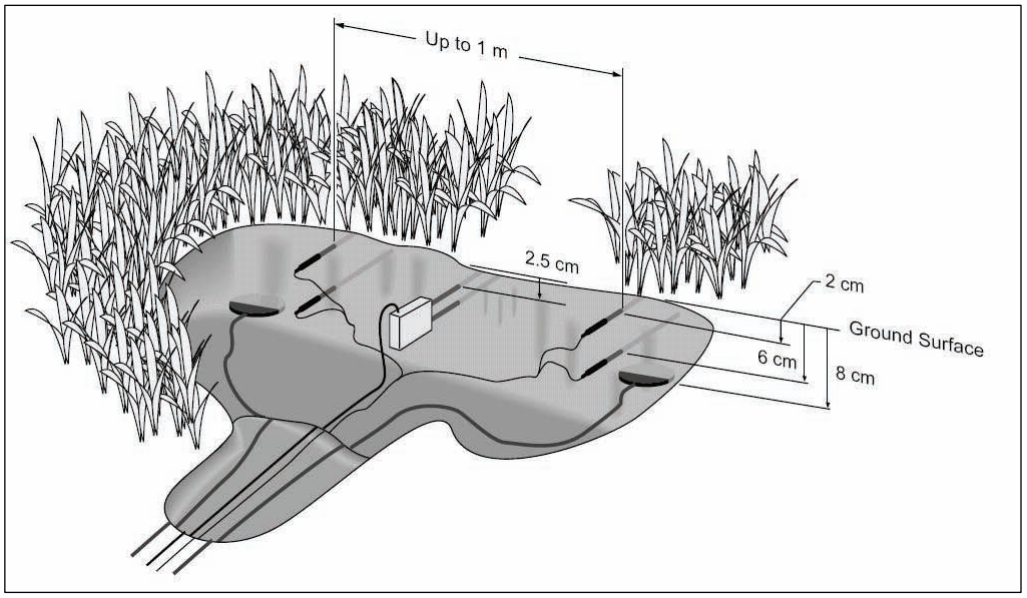

Figure 6.4. Layout of sensors used to estimate soil heat flux (Campbell, 2003).

The net irradiance was stored directly in the logger memory. Soil heat flux was calculated in an Excel spreadsheet using the ten minute data from the soil heat flux plates, the soil temperature averaging probes and the Campbell Scientific CS616 volumetric soil-water reflectometer using Equations 6.1 and 6.2.

$F_s = F_{plate} + F_{stored}$	*6.1*

$F_{stored} = \frac{\rho_s \, \Delta T_s \, c_s \, d}{\Delta t}$	*6.2*

where F_s is the soil heat flux at the surface (W m^{-2}), F_{plate} is the heat flux at a depth of 80 mm (W m^{-2}), F_{stored} is the flux of heat storage in the soil (W m^{-2}), ρ_s is the bulk density of soil (kg m^{-3}), ΔT_s is the temporal change in temperature over the output interval (K), c_s is the specific heat capacity of soil (J kg^{-1} K^{-1}), d is the depth of the heat flux plates in the soil (m) and Δ_t is the output time interval (s).

7. Results

7.1 Early Summer (14-22 October 2007)

7.1.1 The energy balance at EWR 3

The diurnal course of the ambient air temperature showed the extreme nature of the climate during this October period, with daily maxima ranging between 29.5°C and 34.5°C and daily minima between 10.6°C and 16.2°C (Figure 7.1). The relative humidity was generally very low during daylight hours (5 to 20%) while night values were also low (20 to 70%) (Figure 7.2). These data illustrate the hot dry conditions experienced during the early summer field campaign.

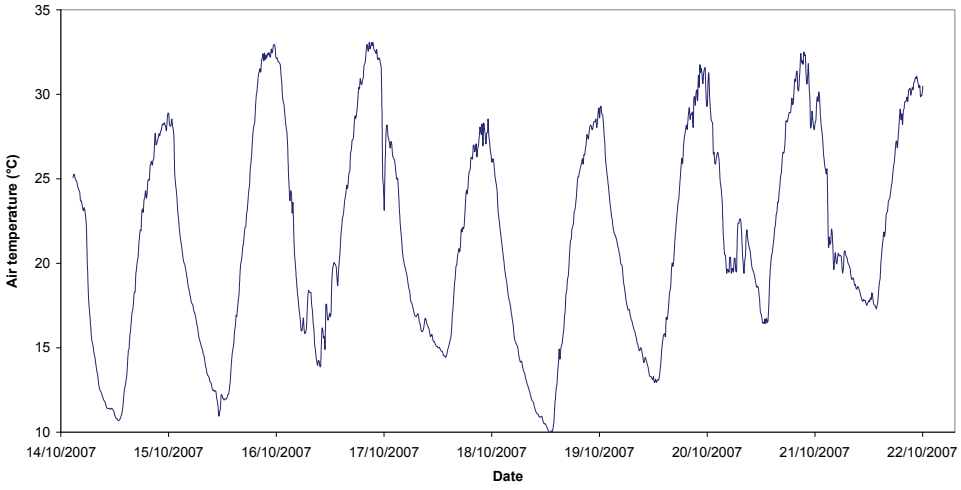

Figure 7.1. Ten minute air temperature in the riparian area during the early summer measurements at EWR site 3.

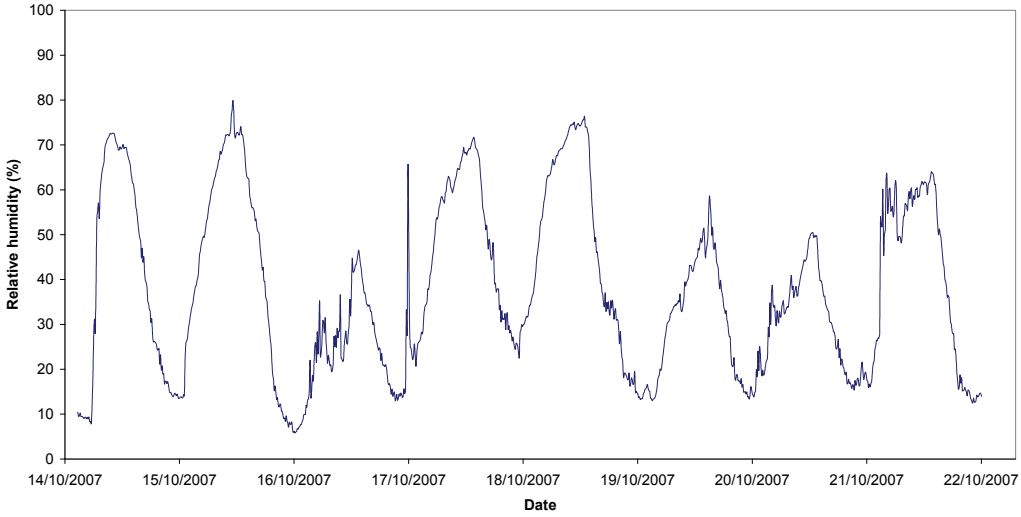

Figure 7.2. Ten minute relative humidity in the riparian area during the early summer 2007 field campaign at EWR site 3.

The solar irradiance showed that the 15th, 16th and 19th of October had perfectly clear days with maximum values of 1000 W m^{-2} recorded at midday (Figure 7.3). These data followed the typical bell shaped curves indicative of cloudless days. The 17th, 18th, 20th and 21st of October were all characterised by intermittent cloud cover as evidenced by the jagged nature of the curves. These intermittent cloudy conditions were more frequent in the afternoon than in the morning (Figure 7.3).

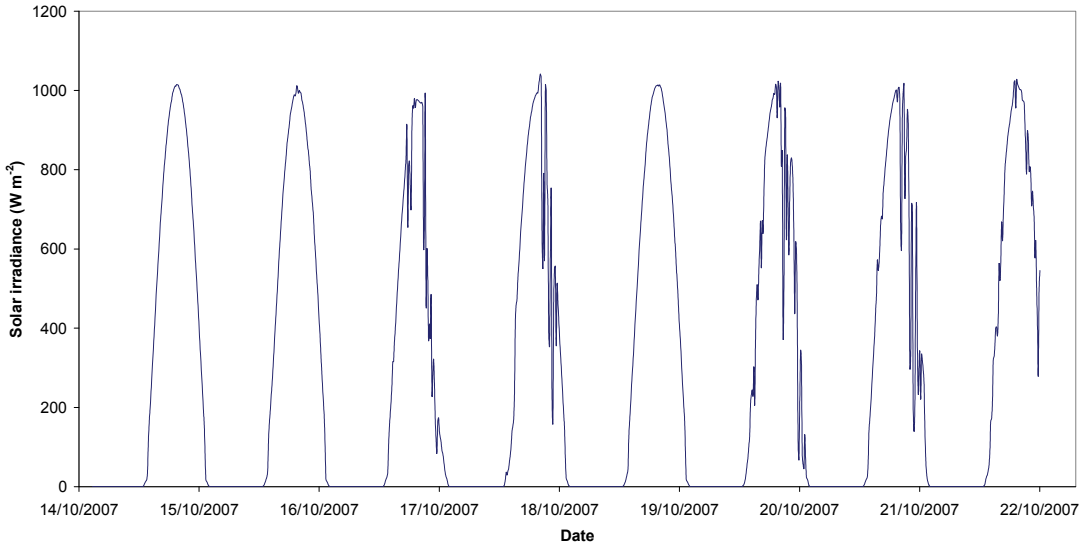

Figure 7.3. Diurnal course of solar irradiance at the EWR site 3 riparian area during the early summer 2007 field campaign.

Two small rain events of 2.4 mm and 0.9 mm were recorded at night on the 17th and 21st October respectively (Table 7.1).

Between the 15th and 21st October total daily solar irradiance averaged 26 MJ day^{-1}, illustrating the high radiation loads experienced at the EWR site 3. This was reflected in the high average maximum air temperature and low minimum relative humidity (32.9°C and 13.2% respectively). Winds averaged 2.0 m s^{-1} and were predominantly from the North-West (Table 7.1). Volumetric soil water content in the top 80 mm of the sandy soil surface was only 9.5% on the 15th October and increased to 9.9% after the 2.4 mm rainfall event on the 17th October. The plants at EWR site 1 were showing signs of the first spring flush of new leaves. Conditions at the site were therefore hot and dry with limited soil water in the upper soil horizon. Thus plants not in contact with the ground water table would be expected to experience plant water stress at this time.

Table 7.1. A summary of the climatic variables measured at EWR site 3 during the early summer 2007 field campaign.

Date	Solar irradiance	Windspeed	Wind direction	Air temperature max			RH		Rain	Vol. soil water
	total	average	average	maximum	minimum	average	maximum	minimum	total	average
	(MJ m^{-2} day^{-1})	(m s^{-1})	(°)	(°C)	(°C)	(°C)	(%)	(%)	(mm)	(%)
15/10/2007	28.2	1.8	13.7	29.5	10.6	19.1	73.3	13.0	0.0	9.5
16/10/2007	27.8	1.7	341.4	33.4	10.7	21.5	80.3	5.5	0.0	9.5
17/10/2007	22.2	2.5	21.1	34.0	13.4	23.6	72.3	11.7	2.4	9.7
18/10/2007	24.7	1.9	10.6	29.2	13.5	19.9	71.9	22.0	0.0	9.9
19/10/2007	28.3	1.7	315.3	29.6	9.7	19.3	76.8	12.7	0.0	9.7
20/10/2007	25.5	1.5	281.0	32.4	12.7	21.7	59.2	13.0	0.0	9.7
21/10/2007	25.6	2.6	273.6	32.9	16.2	24.0	66.2	14.7	0.9	9.7
Mean	**26.0**	**2.0**		**31.6**	**12.4**	**21.3**	**71.4**	**13.2**		**9.7**

The stage height at the main pool was only 0.7 m and the depth to the ground water table at boreholes 1, 2 and 3 was 7.8, 2.9 and 6.8 m below the ground surface respectively. The plants on the upper levee may therefore not have had access to free water at this time of year. Root distribution or tracer studies would be required to confirm these observations.

The diurnal course of the energy balance components from the 15th to the 22nd of October are shown in Figure 7.4, while a typical cloudless day (19th October) is shown for clarity in Figure 7.5. Net radiation peaked at ± 700 W m^{-2} at midday on most days. The sensible heat flux followed the net radiation but was lagged with maximum values of 300-350 W m^{-2} being recorded between 12h00 and 13h00. The soil heat flux was generally high (± 180 W m^{-2}) in the first half of the day, where after it decreased rapidly to low and negative values after 14h00 (Figures 7.4 and 7.5). This response of the soil heat flux is interpreted as being a result of the large percentage of bare ground at the site, combined with the effect of shading by the trees in the early and late afternoon.

The sensible and latent heat fluxes were generally equally partitioned in the morning (Bowen ratio = 1) (Figure 7.5). In the afternoon the latent heat flux dominated the energy balance (Bowen ratio < 1) as a result of the simultaneous decrease in the soil heat flux at this time.

The total daily evaporation for the period 15th to 22nd October 2007 varied between a low of 2.1 mm day^{-1} on a cloudy day to 3.2 mm day^{-1} on a hot clear day (19th October 2007). The average evaporation for the eight recorded days was 2.77 mm day^{-1} (Figure 7.6). The FAO-56 short grass reference evaporation during this early summer filed campaign was 5.7 mm day^{-1} (Figure 7.6), approximately double the actual evaporation from EWR site 3 during the same period.

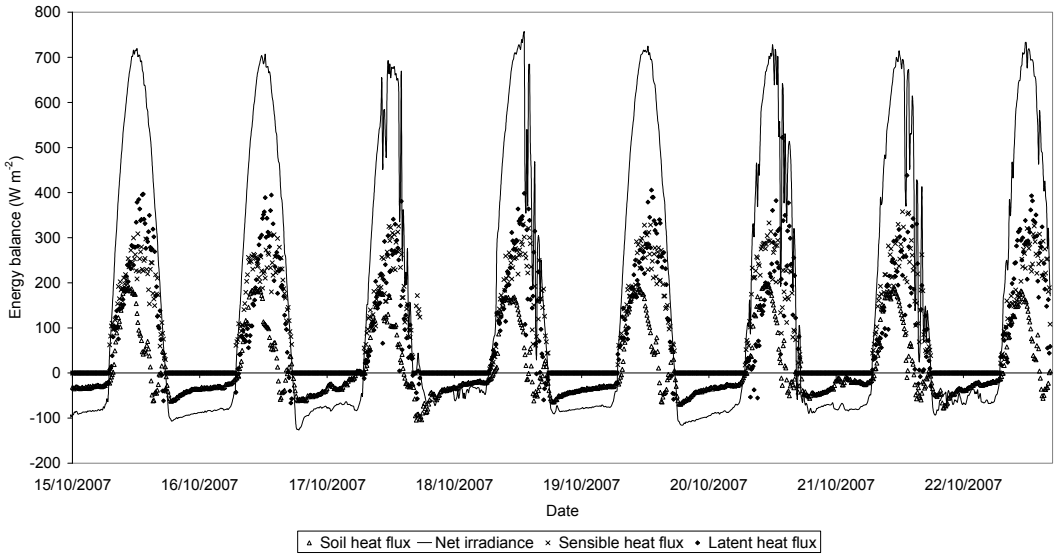

Figure 7.4. Components of the energy balance in the riparian area during the early summer 2007 field campaign at EWR site 3.

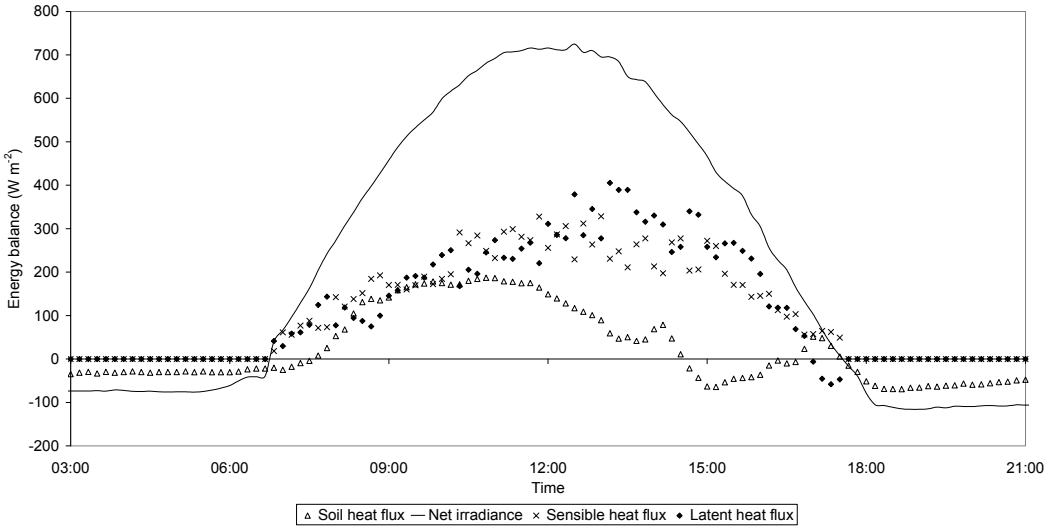

Figure 7.5. The energy balance components for a typical cloudless day at the EWR 3 site on the 19th October 2007.

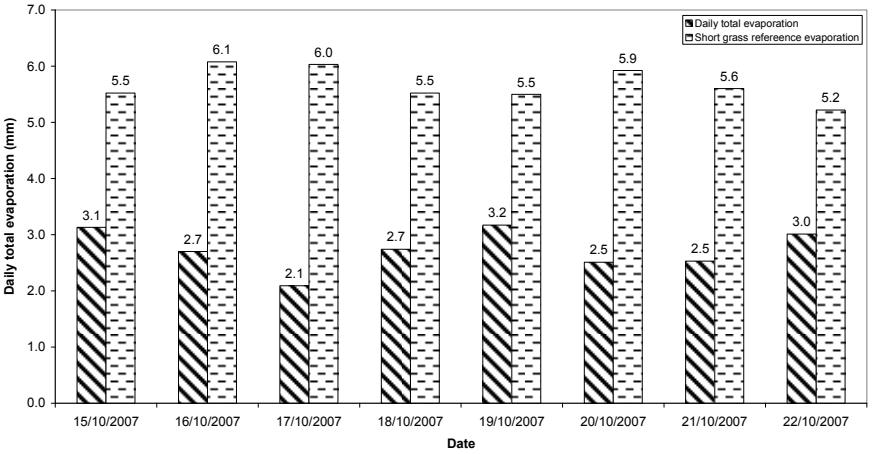

Figure 7.6. Daily total evaporation and FAO-56 short grass reference evaporation in the early summer 2007 field campaign at EWR site 3.

7.1.2 The energy balance at the EWR 1"dry veld" and riparian sites

Due to the complex nature of the site setup it took two full days to install the two OEBMS1 systems at EWR site 1. The installation was further complicated by technical difficulties found with one of the receiver units. We were able to collect good energy balance data from the dry veld site (five days) and riparian site (six days) between the 15th and the 20th of October 2007.

Solar irradiance was high with maximum values approaching 1000 W m^{-2} at midday. Two cloudless days occurred on the 17th and 18th while the remaining days had varying degrees of intermittent cloud cover (Figures 7.7 and 7.8). Net radiation peaked at midday but was consistently higher (±100 Wm^{-2}) at the riparian site than over the dry veld. This can be seen more clearly in the comparison of the energy balance components on a cloudless day at both sites on the 17th October (Figure 7.9). Both OEBMS1 systems had two component net radiometers and the data for the outgoing radiation (both longwave and shortwave) was significantly higher at the dry veld site than for the riparian zone (data not shown here). Clearly the reflection of radiation was higher at the dry veld site than the riparian site, resulting in more outgoing longwave and shortwave radiation (i.e. lower net radiation over the dry site). It is important to note that the two net radiometers were only 35 m apart so that no differences in the incoming radiation were expected. Since some small differences were found, all the radiation sensors were carefully recalibrated against known standards back in Pietermaritzburg in January 2008. The new calibration equations were then applied to the raw data and all the radiation components recalculated to correct any anomalies. We are therefore confident that the radiation data presented in this report are of a high standard.

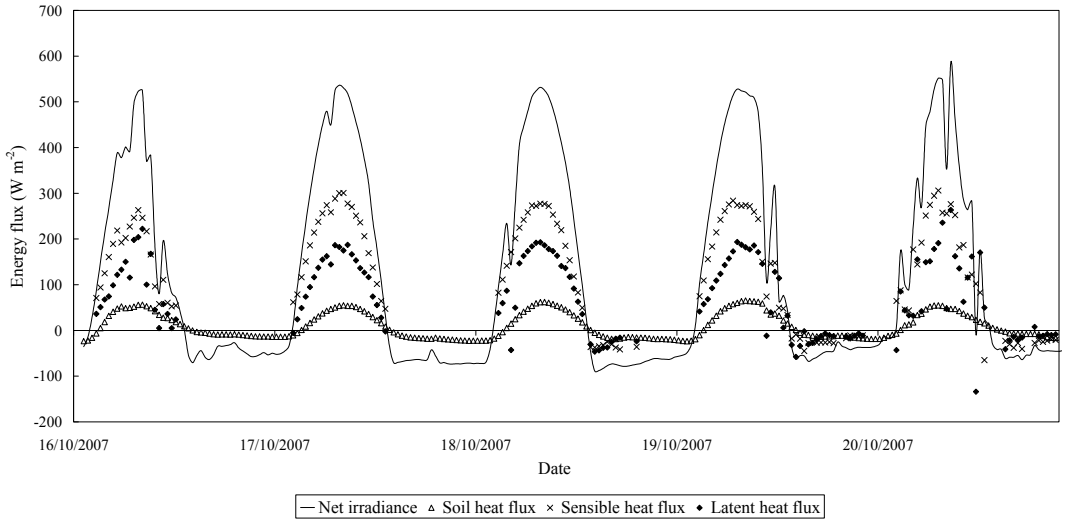

Figure 7.7. Energy balance components of the dry veld at EWR site 1 during early summer (October 2007).

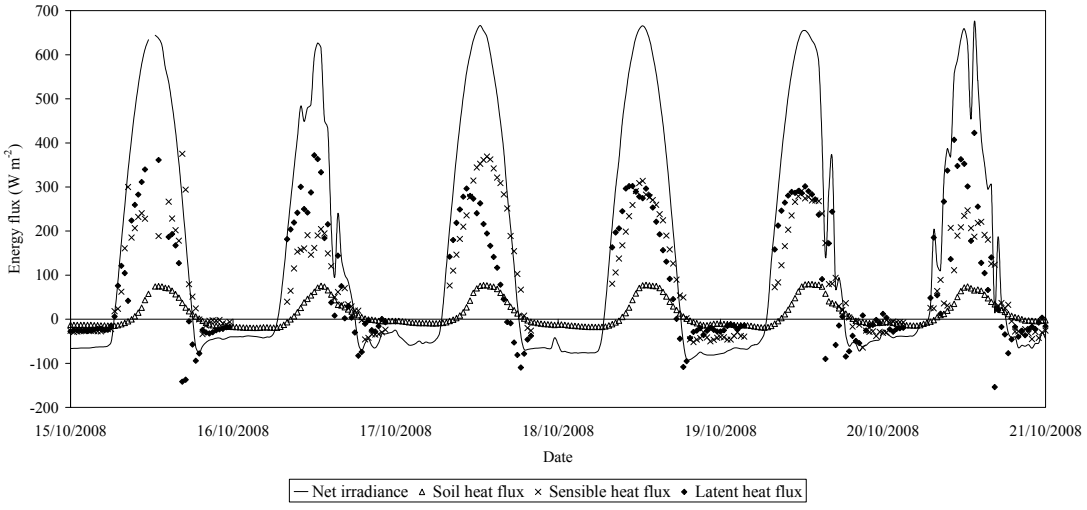

Figure 7.8. Energy balance components of the riparian zone at EWR site 1 during early summer (October 2007).

The magnitude of the soil heat flux at both sites was similar at the riparian and veld sites (maximum ± 77 and 65 Wm^{-2} respectively). However in the more open dry veld site the soil heat flux closely followed the pattern of the net radiation, becoming positive at 08h00 and only becoming negative again at 17h30. By contrast the soil heat flux at the riparian site only became positive at about 09h30, a direct result of the increased shading by the taller and denser *Juncus* canopy. At midday the soil heat flux at the riparian site was generally higher than the veld site by ± 15 Wm^{-2}. These small compensating differences meant that the daily differences (sum of all positive values) in the soil heat fluxes were generally less than 1%. It is clear that the lower R_n at the veld site results in less available energy (R_n -F_s) at this site than at the riparian site.

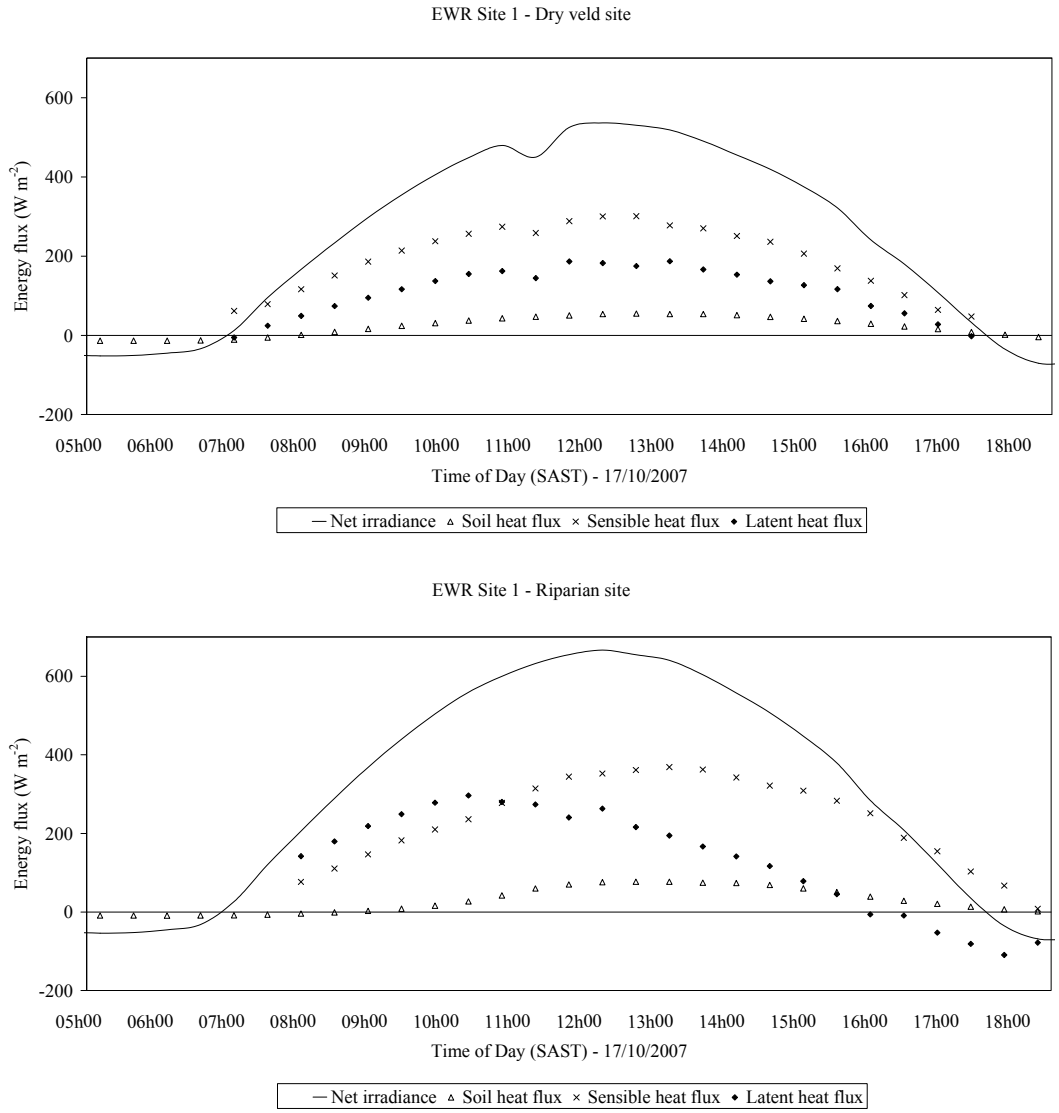

Figure 7.9. The energy balance components for a typical cloudless day at the EWR 1 site over the dry veld and riparian zone on the 17th October 2007.

The sensible heat flux at both sites was similar peaking at ± 300-350 Wm^{-2} at midday (Figures 7.7 to 7.9). An X-Y scatter plot with a linear regression showed that the slope was 0.95 (R^2 = 0.82), confirming the similarity in the sensible heat flux between the two sites (Figure 7.10). The magnitude of the latent heat flux is equal to the flux between the available energy and sensible heat flux. At the dry veld site the trend in the latent heat flux was similar to both the net radiation and sensible heat flux (Figures 7.7 to 7.9). However during the middle of the day the latent heat flux was significantly lower than the sensible heat flux by ± 100 Wm^{-2} (i.e. β=>1). By contrast the latent heat flux at the riparian site was generally higher than the sensible heat flux in the early morning (β=<1). These graphs also showed that the magnitude of the latent heat fluxes was much larger at the riparian site than at the dry veld site (Figures 7.1 to 7.3).

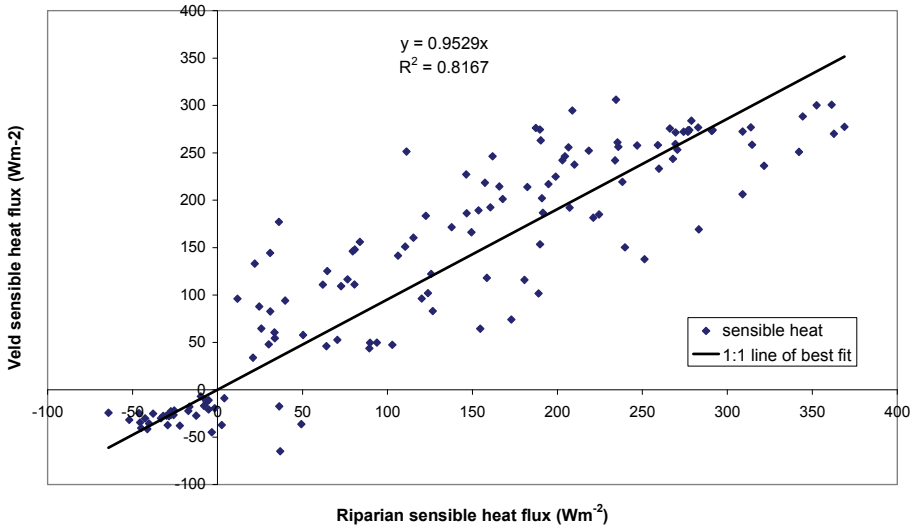

Figure 7.10. A comparison of the sensible heat flux at the veld and riparian sites at the EWR site 1 in October 2007.

The daily totals of evaporation for each site and the differences between them showed large dissimilarities between sites, with the dry veld site ranging between 1.4-1.9 mm day^{-1} (mean = 1.78 mm) and the riparian site 2.5-3.1 mm day^{-1} (mean 2.77 mm) (Figure 7.11). This resulted in a mean site difference of 1.13 mm day^{-1} between the 17th and 21st of October.

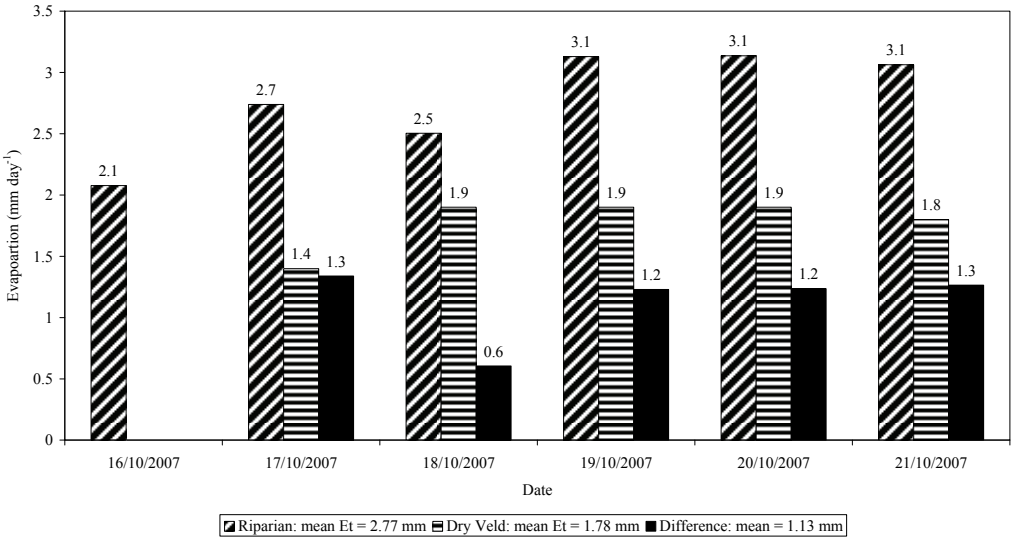

Figure 7.11. A comparison between the results from the adjacent riparian and dry veld sites showing the differences in the daily total evaporation and 21st of October.

These results showed that the riparian water usage in the upper reaches of the Seekoei River was 65% higher than the surrounding dry veld following the prolonged drought period in October 2007. These differences were a direct result of the higher available energy at the riparian site than at the dry veld site. The average evaporation for EWR site 1 riparian zone (2.77 mm day^{-1}) was surprisingly identical to that measured at the EWR site 3 riparian site (2.77 mm day^{-1}).

7.2 Summer (41-5 February 2008)

7.2.1 The energy balance at EWR 3

The first three days of the summer field campaign were hot, with midday temperatures approaching 33°C, relative humidity below 20% and solar irradiance > 1100 Wm^{-2} (Figures 7.12-7.14). However the next four days (9^{th} to 13^{th}) were characterized by a major rainfall event, created by a cut-off low situated over the north western parts of Southern Africa. This brought cool cloudy conditions with regular scattered thundershowers. At the EWR 3 site 24.9 mm was recorded but significantly higher falls (> 50 mm) were reported at Colesberg and Hanover. An assessment of the rainfall for November 2007 to January 2008 showed that the study area received above normal rainfall in the period prior to the summer field campaign (Figure 7.15).

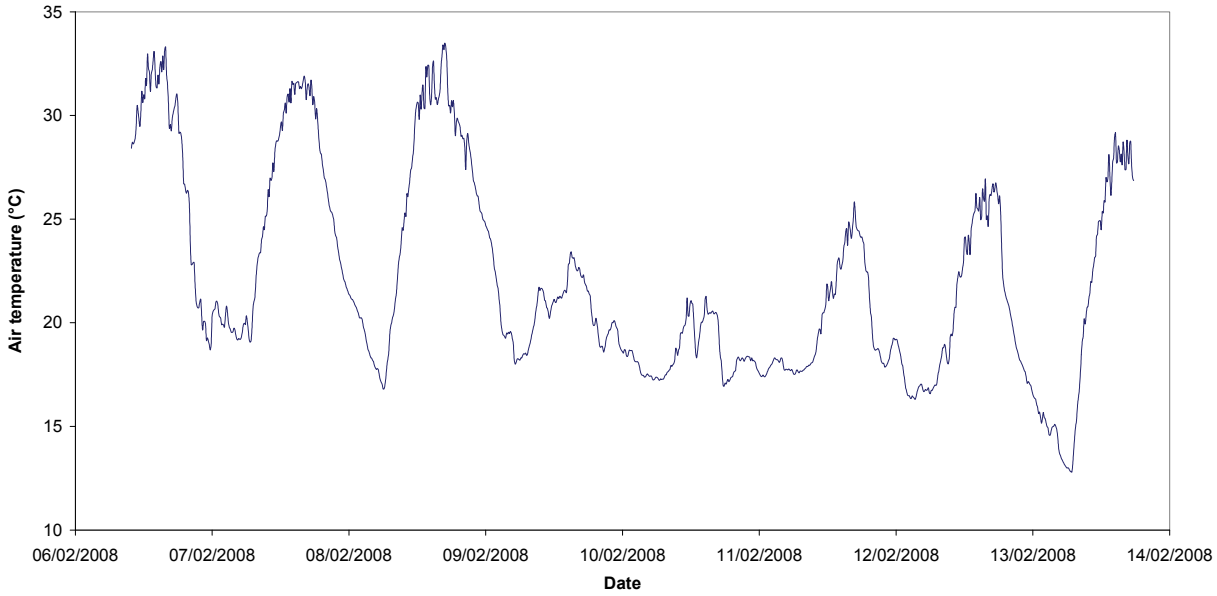

Figure 7.12. Ten minute averaged air temperature data in the riparian area during the summer measurements at EWR site 3.

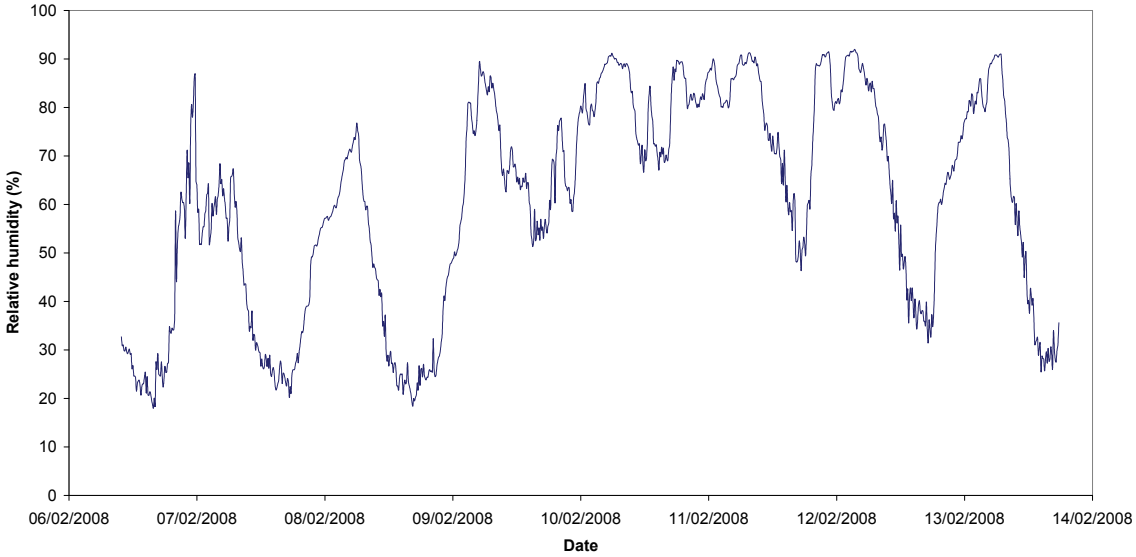

Figure 7.13. Ten minute relative humidity data in the riparian area during the summer 2008 field campaign at EWR site 3.

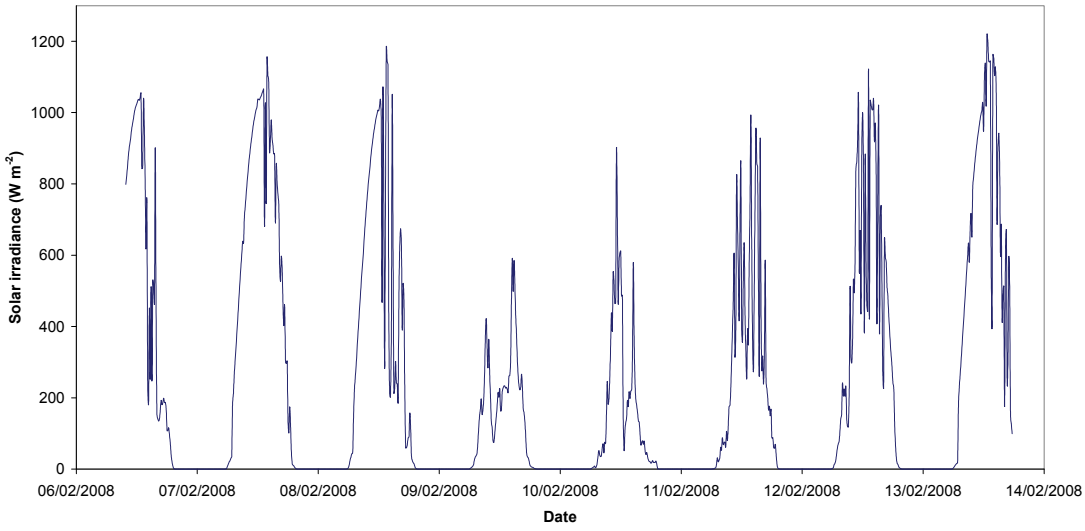

Figure 7.14. Ten minute solar irradiance data in the riparian area during the summer 2008 field campaign at EWR site 3.

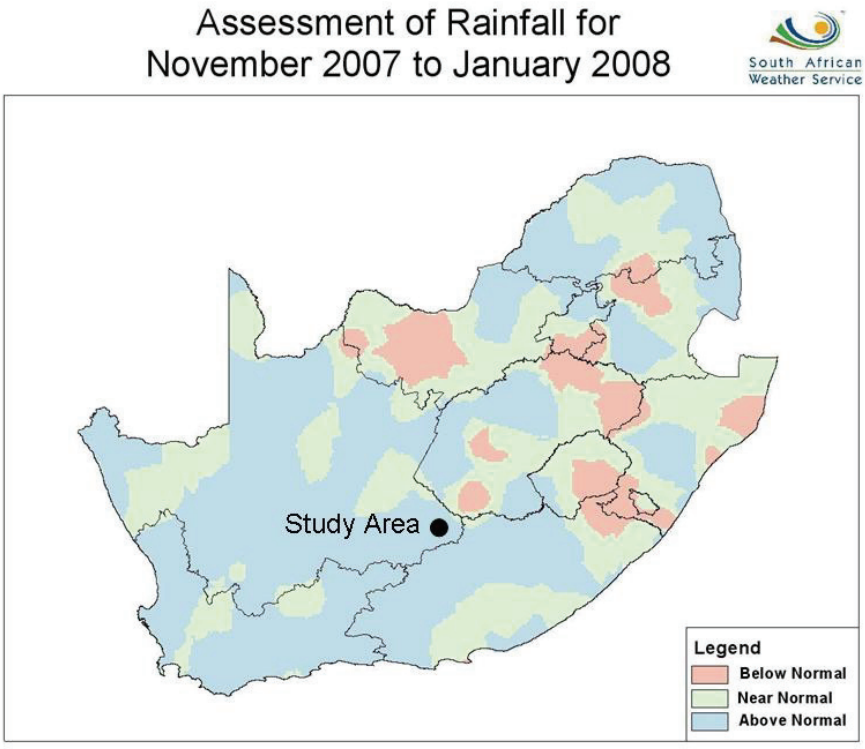

Figure 7.15. An assessment of the rainfall in SA for November 2007 to January 2008.

Since the study area experienced severe drought in the period prior to November 2007 the two field campaigns provided a rare opportunity to compare both very dry and very wet events.

Between the 6th and 12th February total daily solar irradiance averaged only 18 MJ day^{-1}, a result of the high percentage of cloud cover experienced at the EWR site 3 (Table 7.2). This was 30% lower than the 26 MJ day^{-1} recorded during the early summer field trip (Table 7.1). The effect of the low solar irradiance was also reflected in the relatively low average maximum air temperature and high minimum relative humidity (28.6°C and 35.0% respectively). This contrasts with the 31.6°C and 21.3% recoded in October 2007. Winds averaged 1.5 m s^{-1} and were predominantly from the North-West (Table 7.2). Volumetric soil water content in the top 80 mm of the sandy soil surface was about 10% on the 6th February and increased to 17.3% following the 24.9 mm of rainfall which fell during the week. Conditions at the site were therefore cool and wet, with adequate soil water in the upper soil horizon. Since the plant canopy was also fully developed, conditions in February 2008 were ideal for measuring high evaporation rates on clear hot sunny days.

Table 7.2. A summary of the climatic variables measured at EWR site 3 during the summer 2008 field campaign.

Date	Solar irradiance	Windspeed	Wind direction	Air temperature max			RH		Rain	Vol. soil water
	total	average	average	maximum	minimum	average	maximum	minimum	total	average
	(MJ m^{-2})	(m s^{-1})	(°)	(°C)	(°C)	(°C)	(%)	(%)	(mm)	(%)
06/02/2008	18.8	1.7	225	33.8	18.5	27.6	88	16	0.9	10.1
07/02/2008	29.9	1.5	341	32.5	18.9	25.2	69	20	0.0	9.9
08/02/2008	24.0	1.5	315	34.0	16.7	25.5	77	18	0.0	9.7
09/02/2008	8.7	1.5	350	24.7	18.0	20.6	90	49	8.8	11.2
10/02/2008	8.8	1.8	273	21.7	16.8	18.5	91	66	5.4	12.3
11/02/2008	14.8	1.4	224	26.3	17.3	19.9	92	45	8.5	16.5
12/02/2008	21.7	0.9	82	27.3	16.2	20.4	92	30	0.3	17.3
Mean	**18.1**	**1.5**		**28.6**	**17.5**	**22.5**	**85**	**35**	**24.9**	**12.4**

The diurnal course of the energy balance components from the 6th to the 14th of February are shown in Figure 7.16, while a typical day (7th February) is shown for clarity in Figure 7.17. Net radiation showed short peaks, >800 W m^{-2} on most hot days (6-8 and 14 February) while maximum values were generally < 600 W m^{-2} on the cloudy days. The large incidence of intermittent sun experienced during the summer filed campaign is shown by the very "jagged" nature of the diurnal data (Figure 7.16).

The sensible heat flux followed the net radiation with maximum values of 400 Wm^{-2} being recorded between 12h00 and 14h00 on the warmer days. The soil heat flux was generally high (± 180 W m^{-2}) in the first half of the day, where after it decreased rapidly to low and negative values after 14h00 (Figures 7.16 and 7.17). This response was similar to that found during the early summer field campaign and was again interpreted as being a result of the large percentage of bare ground at the site, combined with the effect of shading by the trees in the early and late afternoon. Because of the high variability in the ground cover it would be important to increase the number of soil heat flux measurements in future studies to obtain a better spatial average. In most studies the soil heat flux represents only about 10% of the energy balance and is easily measured in closed canopy situations. In this study the soil heat flux was 25% of the net irradiance, highlighting its importance in semi-arid conditions.

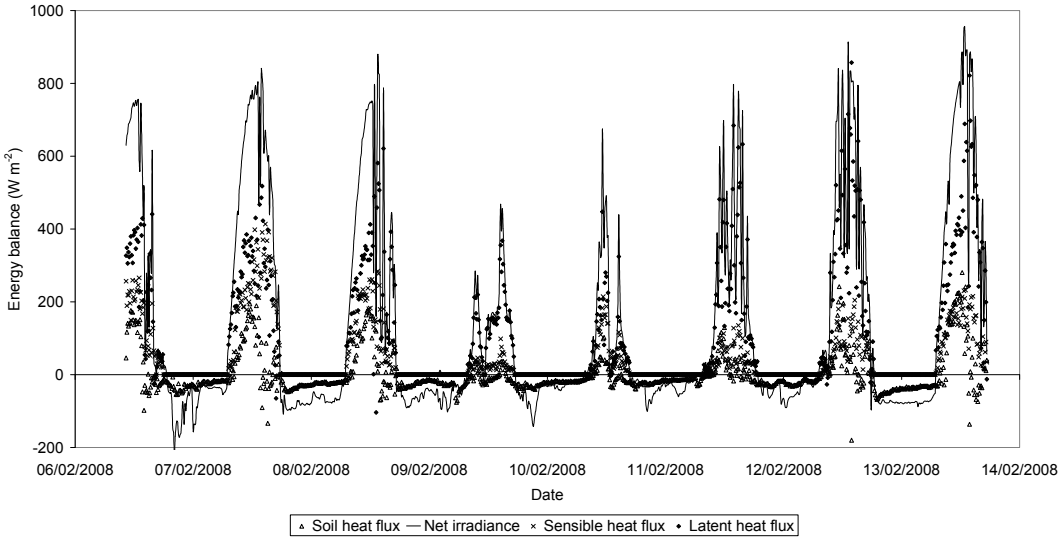

Figure 7.16. Components of the energy balance in the riparian area during the summer 2008 field campaign at EWR site 3.

The sensible heat flux was generally less than the latent heat flux in the morning (Bowen ratio = <1), showing the dominance of evaporation at this time (Figure 7.16 and 7.17). In the afternoon the sensible and latent fluxes equally dominated the energy balance (Bowen ratio = 1) as a result of the simultaneous decrease in the soil heat flux at this time.

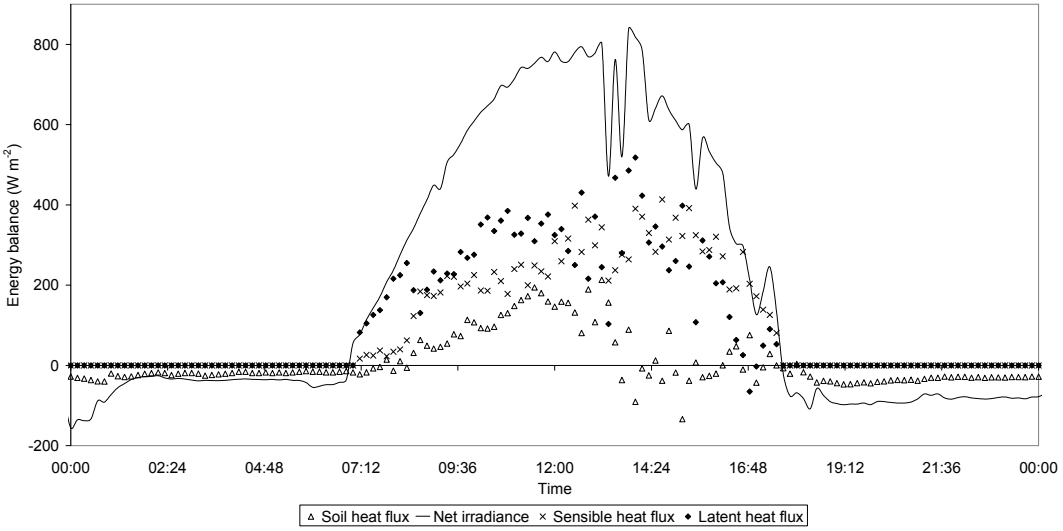

Figure 7.17. Energy balance components for the 7 February 2008 for EWR site 3.

The total daily evaporation for the period 6th to 13th October 2007, varied between a low of 1.3 mm day^{-1} on a cloudy and wet day, to 5.2 mm day^{-1} on a hot clear day after the good rains (13th February 2008). The average evaporation for the eight recorded days was 3.3 mm day^{-1} (Figure 7.18). The FAO-56 short grass reference evaporation during this early summer filed campaign averaged 3.9 mm day^{-1} (Figure 7.6). The LAS and FAO 56 values were similar on the cool wet days, but interestingly the FAO 56 reference evaporation was much higher on the dry hot days preceding the rain event. For example on the 7th the

FAO 56 was 6.8 mm compared to the 3.9 mm measured with the LAS. The maximum daily total evaporation in the early summer was only 3.1 mm compared with the 5.2 mm recorded in summer. This is clearly a result of the more favourable conditions for evaporation during the unusually wet summer campaign.

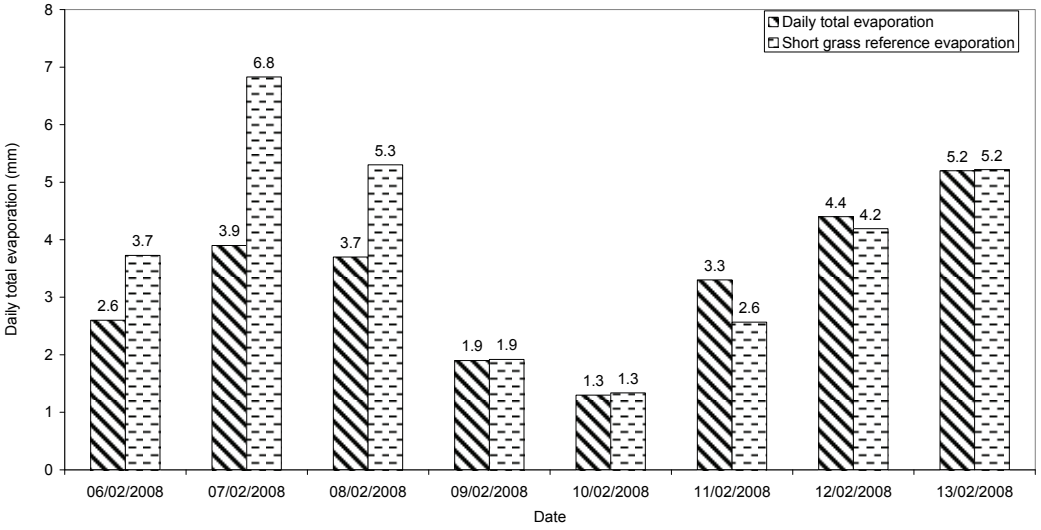

Figure 7.18. Daily total evaporation using a large aperture scintillometer and daily FAO-56 short grass reference evaporation in the summer 2008 field campaign at EWR site 3.

7.2.2 The energy balance at the EWR 1"dry veld" and riparian sites (Summer 2008)

The diurnal course of the energy balance components for the summer field campaign showed that the first three days were hot with maximum net radiation at both the riparian and dry sites of ± 720 W m^{-2} (Figures 7.19 and 7.20). The soil heat fluxes on these hot days were about 50 W m^{-2} in the dry and riparian sites respectively, and were not noticeably different. The sensible heat flux at both sites was relatively low, peaking at about 200 and 100 Wm^{-2} in the dry and riparian sites respectively. The energy balance at both the dry and riparian sites was dominated by the latent heat flux which closely followed the diurnal trends in the net radiation with maxima of about 520 and 400 Wm^{-2} in the dry and riparian sites respectively (Figures 7.19-7.21). This resulted in the total evaporation rates on the 06 to 07 February 2008 exceeding those at the dry site by about 1.5 mm day^{-1} (Figure 7.22). The arrival of the cooler wet weather on the 9th February had a significant effect on the energy balance with the net radiation dropping below maxima of 400 Wm^{-2}, resulting in daily evaporation of < 2 mm day^{-1}. There was a gradual recovery in these rates as the weather warmed over the next five days. Unfortunately technical problems resulted in a loss of data from the riparian site during these five days so no direct comparisons were possible. However by the 14th on February the total evaporation at the riparian site was 5.4 mm and only 4.3 mm at the dry site. These data showed that the evaporation rates from the riparian area during summer were consistently higher by 1.1 to 1.8 mm during the study period (Figure 7.22). The summer period evaporation rates were about 2 mm day^{-1} higher than those measured during the "dry" early summer field campaign.

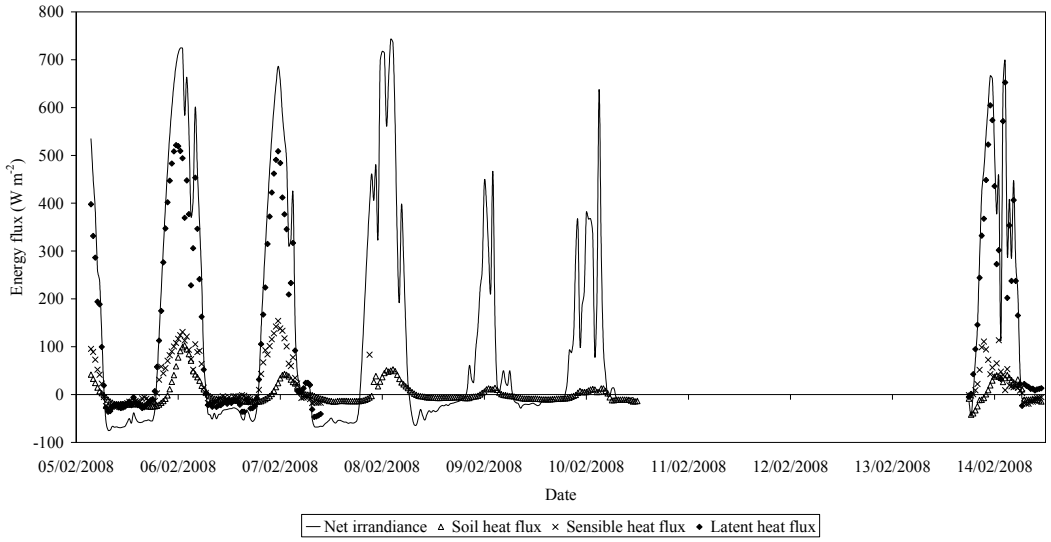

Figure 7.19. Energy balance components of the dry veld EWR site 1 during summer field campaign.

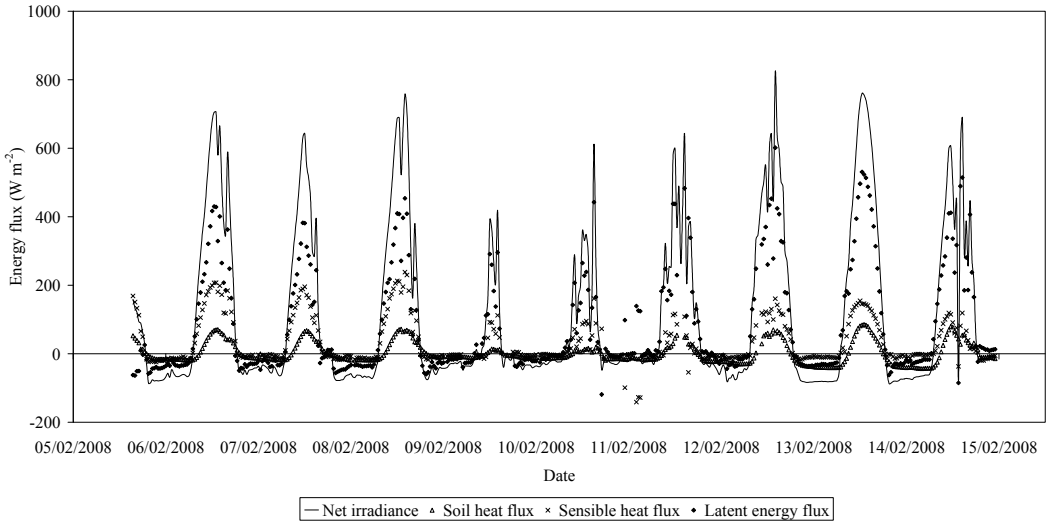

Figure 7.20. Energy balance components of the riparian EWR site 1 during summer field campaign.

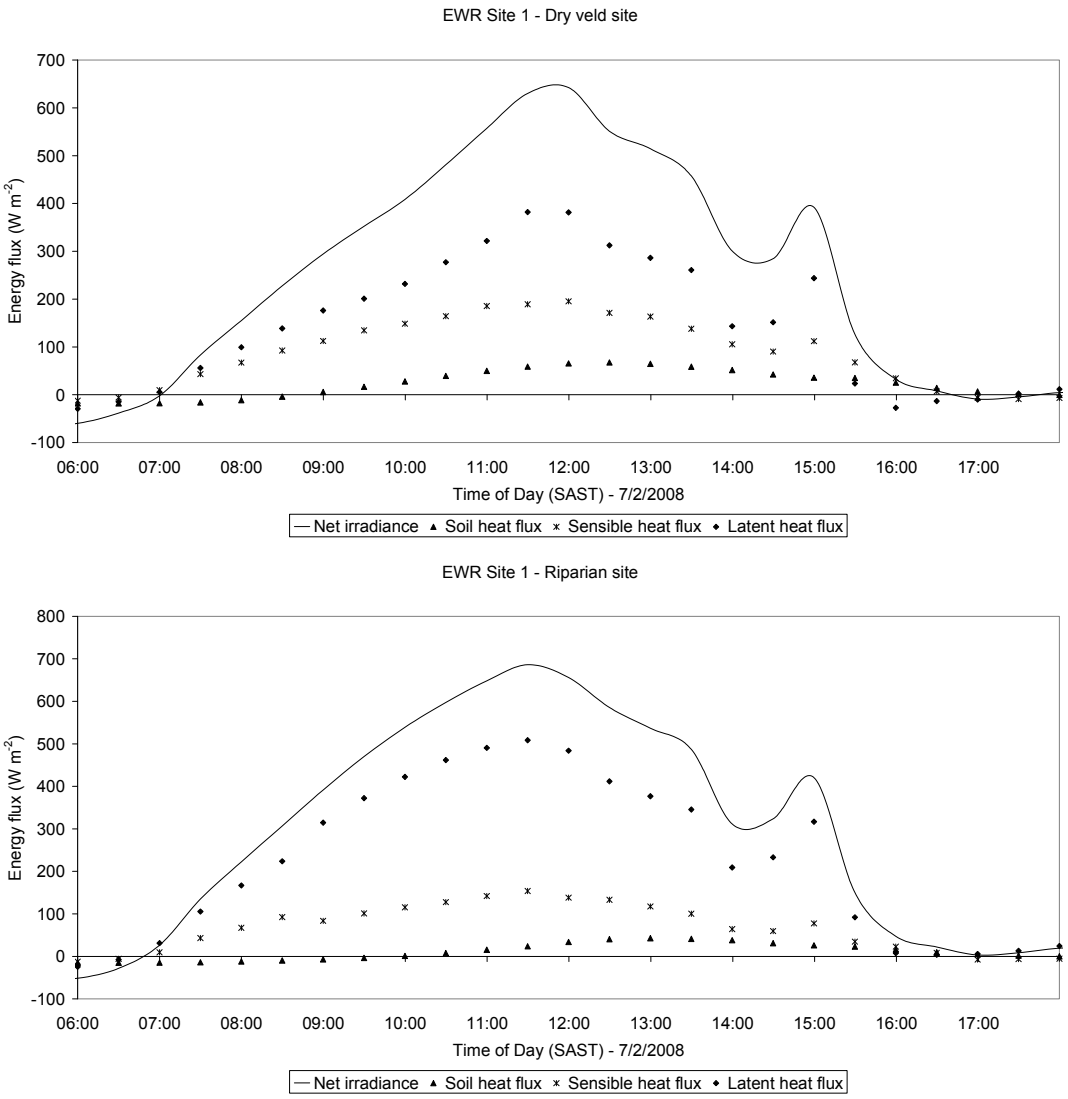

Figure 7.21. A comparison of the energy balances for the EWRI site 1 dry veld and riparian sites on the 7 February 2008.

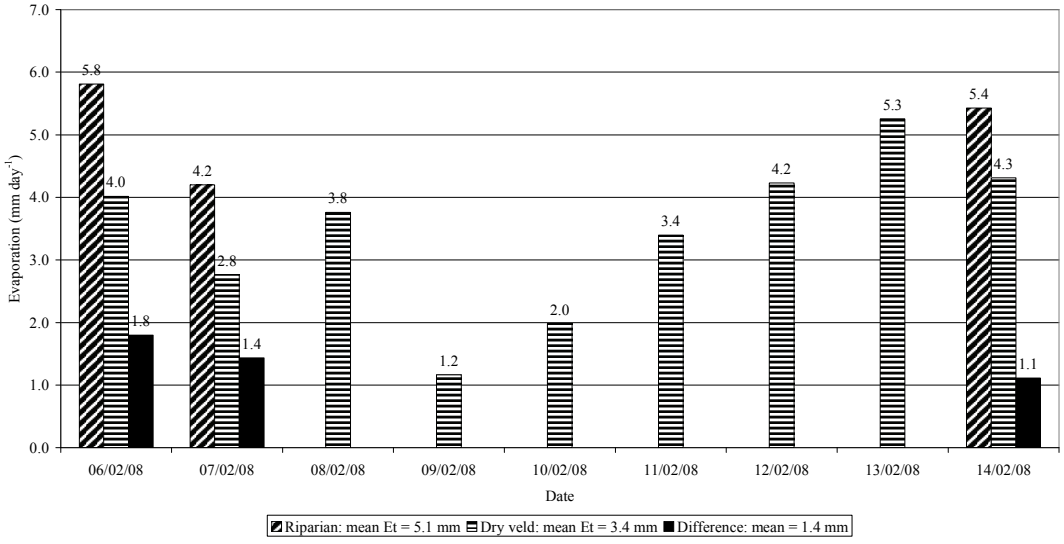

Figure 7.22. A comparison between the results from the adjacent riparian and dry veld sites showing the differences in the daily total evaporation for the summer field campaign at EWR site 1.

8. Conclusions

This study was initiated to test the feasibility of measuring riparian evaporation in the semi arid karoo vegetation in the dry regions of the Free State and Eastern Cape. The aim was to estimate early summer and summer evaporation rates from three distinct vegetation types (two riparian and one dryland). The two field campaigns have shown that there are distinct site and seasonal differences between the three different canopies measured. Although there was some data loss at Hanover, a large data base of climatic and energy flux data, comprising some 30 days of two minute and ten minute data have been gathered.

The results have shown both significant plant community and seasonal differences which will provide the modelling team with valuable insights into the evaporation processes along the Seekoei River. The early summer period at the EWR 3 site was characterised by very hot and dry conditions. The average evaporation for the eight recorded days was only 2.77 mm day^{-1} and contrasts with the FAO-56 reference evaporation of 5.7 mm day^{-1} (double the actual evaporation). The soil heat flux was generally high (± 180 W m^{-2}) and a significant component of the energy balance, representing about 30% of the available energy in the morning. This response of the soil heat flux is interpreted as being a result of the large percentage of bare ground at the site, combined with the effect of shading by the trees in the early and late afternoon.

Riparian water usage in the upper reaches of the Seekoei River was 65% higher than the surrounding dry veld following the prolonged drought period in October 2007. These differences were a direct result of the higher available energy at the riparian site than at the dry veld site. The average evaporation for EWR site 1 riparian zone (2.77 mm day^{-1}) was surprisingly identical to that measured at the EWR site 3 riparian site (2.77 mm day^{-1}).

In the summer period the conditions at the EWR3 site were cool and wet, with adequate soil water. The maximum daily total evaporation was 5.2 mm compared to only 3.1 mm in the early summer period. The summer soil heat flux was high (± 180 W m-2) in the first half of the day, decreasing rapidly after 14h00 results similar to those found in the early summer field campaign.

At site EWR1 the evaporation rates from the riparian area during summer were consistently higher by 1.1 to 1.8 mm and about 2 mm day^{-1} higher than those measured during the "dry" early summer field campaign. The sensible heat fluxes at both sites were relatively low, at about 200 and 100 Wm-2 in the dry and riparian sites respectively. This was clearly a result of the more favourable conditions for evaporation during the unusually wet summer campaign when the energy balance at both the dry and riparian sites was dominated by LE.

In most studies the soil heat flux represents only about 10% of the energy balance. In this study the soil heat flux was 25% of the net irradiance, highlighting its importance in semi-arid conditions. Because of the high variability in the ground cover it would be important to increase the number of soil heat flux measurements in future studies to obtain a better spatial average.

9. Acknowledgements

This project was designed to support larger projects (K5/1587 and K5/1414) being undertaken for the WRC by the University of the Free State entitled 'Environmental Requirements in Non-Perennial Systems'. The objective of the larger project was to develop methods for determining the environmental water requirements of non-perennial systems. In this respect the significant contributions to this project by Prof. Maitland Seaman and Marinda Avenant from the Centre for Environmental Management at UFS are gratefully acknowledged.

This project would not have been possible without the cooperation of the two landowners on whose farms the research was carried out. We would like to say special thanks to "Oom" Carools and Aletta Venter of the farm Holfontein and to Mr. T.C. Niewhoudt of the farm Vanzylskraal for their kind help during the field campaigns.

As this project was a consultancy there was no Reference Group or Steering Committee appointed. The authors would, however like to acknowledge the contributions of Dr Steve Mitchell, the WRC research manager in charge of the project.

10. References

Avenant, M., 2006. Selection of Sampling Sites on The Seekoei River. Deliverable 3: Exploratory visit to prospective field sites. Environmental Requirements in Non-perennial Systems. WRC Contract No. 1587.

Campbell Scientific, 2003. Instruction manual: *HPT3 soil heat flux plate*. Campbell Scientific Inc., Logan, Utah, USA, 12pp.

Hartogensis O K, Watts C J, Rodriguez J-C, de Bruin H A R, 2003. Derivation of an effective height for scintillometers: La Poza experiment in Northwest Mexico, *American Meteorological Society*, 4, 915-928.

Hughes, DA (2007). Simulating the hydrology and TDS of ephemeral rivers for the purpose of environmental water determinations. Paper presented at the 13th South African National Hydrology Symposium, Cape Town, Sept. 2007.

Kipp and Zonen, 2007. Instruction Manual to the Large Aperture Scintillometer, Delft, Holland, 74pp

Meijninger W M L, Hartogensis O K, Kohsiek W, Hoedjes J C B, Zuurbier R M, de Bruin H A R, 2002. Determination of area-averaged sensible heat fluxes with a large aperture scintillometer over a heterogeneous surface – Flevoland field experiment, *Boundary-Layer Meteorology*, 10, 63-83.

Monin A S, Obukhov A M, 1954. Basic laws of turbulent mixing in the ground layer of the atmosphere, *Tr. Goefiz. Institute Akad*. Nauk. SSSR. 24 (151), 163-187.

Monteith J L, Unsworth M, 1990. *Principles of Environmental Physics*. 2nd ed., Edward Arnold, London, UK, 291pp.

Odhiambo G O, 2007. Long-term measurements of spatially averaged sensible heat flux for a mixed grassland community, using surface layer scintillometry. PhD thesis, University of KwaZulu-Natal, Pietermaritzburg, South Africa.

Rosenberg N J, Blad B L, Verma S B, 1983. *Microclimate: The Biological Environment*, 2nd ed., John Wiley and Sons Inc., New York, 495pp.

Savage M J, Everson C S, Odhiambo G O, Mengistu M G, Jarmain C, 2004. Theory and practice of evaporation measurement, with a special focus on SLS as an operational tool for the estimation of spatially-averaged evaporation, Water Research Commission Report No. 1335/1/04. ISBN 1-77005-247-X, Pretoria, South Africa, 204pp.

Schulze, 1965 in Rutherford , M.C. and Westfall, R.H., 1994. Biomes of southern Africa: an objective classification. Mem. Bot. Surv. S. Afr. No. 63.

Venter, J.M., Mocke, C. & De Jager, J.M. 1986. Climate. In: Karoo Biome: a preliminary synthesis. Part 1 – physical environment. Cowling, R.M., Roux, P.W. & Pieterse, A.J.H. (eds). South African National Scientific Programmes Report No. 124. Pretoria. 115pp.

Verhoef A, McNaughton K G, Jacobs J F G, 1997. A parameterization of momentum roughness length and displacement height for a wide range of canopy densities, *Hydrology and Earth Sciences*, 1, 81-91.

Watson, M. & Barker, C.H. 2006. Habitat integrity assessment of the Seekoei River. Draft report. Prepared for Centre for Environmental Management, Faculty of Natural & Agricultural Sciences, University of the Free State, Bloemfontein. Environmental water requirements in non-perennial systems. Water Research Contract No. 1587.

Wang T I, Ochs G R, Clifford S F, 1978. A saturation resistant optical scintillometer to measure C_n^2, *Journal of Optical Society of America*, 69, 334-338.

Wesley M L, 1976. The combined effect of temperature and humidity on the refractive index, *Journal of Applied Meteorology*, 15, 43-49.

Wyngaard J C, Izumi Y, Collins S A, 1971. Behaviour of the refractive index structure parameter near the ground, *Journal of Optical Society of America*, 61, 1646-1650.